Appendix - Supplementary Information

Structure of a lipid A phosphoethanolamine transferase suggests how conformational changes govern substrate binding

Anandhi Anandan, Genevieve L. Evans, Karmen Condic-Jurkic, Megan L. O'Mara, Constance M. John, Nancy J. Phillips, Gary A. Jarvis, Siobhan S. Wills, Keith A. Stubbs, Isabel Moraes, Charlene M. Kahler and Alice Vrielink*

*correspondence to – alice.vrielink@uwa.edu.au

SI Materials and Methods

Plasmid construction, recombinant protein expression and purification. The gene encoding *Nm*Ept*A*, was amplified by PCR from Nm strain NMB genomic DNA and cloned into the plasmid pTrc99A(1) to create a high copy expression vector with a C terminal hexahistidine tag (pCMK526) (2). For expression of the full length *Nm*EptA the constructed plasmid, pCMK526 was transformed into Escherichia coli strain BL21(DE3)pLysS. Transformants were selected for by the inclusion of ampicillin (50 $\mu g \cdot mL^{-1}$) and chloramphenicol (34 $\mu g \cdot mL^{-1}$) on Luria Broth (LB)/agar plates. A starter culture was prepared by inoculating a single colony into 100 mL LB medium containing the above antibiotics and grown at 37°C overnight. A sufficient volume of the starter culture was used to inoculate 1 L Terrific Broth such that the starting absorbance at 600 nm (OD_{600}) was approximately 0.1. Cells were grown at 37°C in a shaking incubator set at 200 rpm until the OD_{600} reached between 1.0 and 1.2. Protein expression was induced by the addition of isopropyl β-D-1-thiogalactopyranoside to a final concentration of 0.4 mM. Incubation was continued at 25°C and 180 rpm for a further 20 hours. The cells were harvested by centrifuging at 12,290 x g for 1 hour at 4°C.

The harvested cells were resuspended in 50 mM sodium phosphate buffer pH 7.5 containing 300 mM sodium chloride, 10 mM imidazole and 1 mM phenylmethylsulfonyl fluoride at 4°C. Between 20 and 30 mL was used for each gram of cell pellet. Lysis was performed using an Emulsiflex C5 high-pressure homogenizer (Avestin). The lysate was centrifuged at 12,290 x g for 20 min at 4˚C to remove the non-lysed cells. Membranes were isolated by further centrifugation of the supernatant at 185,511 x g for 1 hour using an ultracentrifuge (Beckman Coulter Optima L-90K). Using a tissue grinder (Wheaton USA), the resultant pellet containing the membrane fraction was resuspended in 18 mL of the above lysis buffer containing 1% DDM. The mixture was then gently rocked at 4°C for 4 hours and centrifuged at 185,511 x g for 1 hour to remove the membrane debris.

The supernatant containing the protein solubilized in detergent micelles was filtered using an 0.2 μm Acrodisc syringe filter (Pall Corporation) and applied onto a HisTrap FF affinity chromtagraphy column (GE Healthcare) equilibrated with binding buffer (50 mM sodium phosphate pH 7.5, 300 mM NaCl, 20 mM imidazole and 0.023 % DDM (3 X critical micelle concentration (CMC)) using an ÅKTApurifier FPLC system (GE Healthcare). The unbound protein was washed from the column with binding buffer until the absorbance at 280 nm reached a steady baseline value. The bound *Nm*EptA was eluted from the column using an increasing gradient of elution buffer (50 mM sodium phosphate pH 7.5, 300 mM NaCl, 500 mM imidazole, 0.023 % DDM). A peak corresponding to *Nm*EptA eluted between 20 % and 30 % elution buffer. The collected eluent fractions were pooled and applied onto a PD-10 desalting column (GE Healthcare), or Desalting HiTrap column (GE Healthcare), equilibrated in 50 mM sodium phosphate pH 7.5, 150 mM sodium chloride and 0.023 % DDM. The eluted protein was applied to a size exclusion chromatography column (SEC, Superdex 200 10/30, GE Healthcare) and eluted with 50 mM Hepes pH 7.0, 100 mM NaCl and 0.023 % DDM. SDS polyacrylamide gel electrophoresis (SDS PAGE) was carried out to assess the purity of the eluted peak fractions. Fractions of pure protein were pooled and concentrated using a 100 kDa molecular weight cut off centrifugal filter unit (Vivaspin 20 MWCO 100 000, GE Healthcare) to 15 - 20 $mg{\cdot}mL^{-1}$ as determined by the absorbance at 280 nm using a calculated molar extinction coefficient for *Nm*EptA (73,980 $M^{-1}\,cm^{-1;}$; calculated based on sequence using ProtParam).

*Nm*EptA was also purified in two other detergents namely FC-12 and Cymal-6. The isolated membranes were solubilized with either 1 % FC-12 or 1 % Cymal-6 in 50mM sodium phosphate buffer, pH 7.5 containing 300 mM NaCl, and 10 mM imidazole to extract *Nm*EptA and purified in the respective detergent following the above protocol with a number of alterations. The buffers for the FC-12 purification contained 0.14 % FC-12 (3 X CMC) instead of DDM and the final buffer consisted of 50 mM Hepes pH 7.5, 150 mM NaCl and 0.14 % FC-12. The buffers for purification of *Nm*EptA in Cymal-6 contained 0.084 % Cymal-6 (3 X CMC) and the final buffer consisted of 50mM Hepes pH 7.0 and 100 mM NaCl containing 0.084 % Cymal-6. The protein was concentrated using 50 kDa molecular weight cut off centrifugal filter units (Vivaspin 20 MWCO 50 000, GE Healthcare).

Crystallization.A suitable protein concentration for crystallization of 20 $mg.mL^{-1}$ *NmEptA* in 50 mM Hepes pH 7.0, 100 mM NaCl and 0.023 % DDM was initially screened for crystals with targeted sparse matrix kits MemSys, MemStart and MemGold (Molecular Dimensions Ltd). Two different ratios of protein:precipitant (µL:µL) were used: 0.1:0.1 and 0.2:0.1. Lead conditions from the initial screens were further optimized using the Additive Screen kit (Hampton Research). Crystallization experiments were performed in hanging drop VDX plates (Hampton Research). Optimized crystallization drops contained 1 µL of protein, 1 µL of crystallization solution (1.8 to 2.0 M ammonium sulphate, 100 mM Hepes pH 7.5 – pH 8.0) and 0.2 µL n-octyl-β-D-glucopyranoside (OG) (to give a final concentration of 17 to 19 mM). The drops were equilibrated at 20 ^{o}C against 1 mL crystallization solution in the reservoir. Rod shaped crystals appeared within approximately 20 days.

X-ray data collection, processing and structure solution. *Nm*EptA crystals used for data collection were cryoprotected by briefly passing them through a solution of 30% glycerol, 2.0 M ammonium sulphate and 100 mM Hepes pH 7.5 and flash cooled in liquid N_2. Diffraction data were collected at the MX2 microfocus beamline, Australian Synchrotron (Melbourne). The diffraction images were indexed, integrated and scaled using the XDS program package(3) and data reduction carried out

using SCALA as part of the CCP4 suite of software.(4) Phases were obtained by molecular replacement using PHASER from the CCP4 package. The soluble domain structure of the *Nm*EptA (PDB accession 4KAV) with all the water molecules and ligands removed was used as the search model structure for molecular replacement.

Iterative cycles of model building using COOT(5) and structure refinement with PHENIX(6) were carried out. The TM domain was modeled by first building the alpha helical backbone structure. The side chains and loop regions were built after multiple cycles of refinement as the density maps improved. The Zn^{2+} metal site was incorporated into the model and two detergent molecules (DDM and OG) fitted into residual electron density. The data collection and structure refinement statistics are summarised in Table S1. The atomic coordinates for the crystal structure of *Nm*EptA has been submitted to the Protein Data Bank under the accession number 5FGN.

Size exclusion chromatography – multiangle light scattering (SEC-MALS). SEC-MALS analysis was performed using a 10/300 GL Superdex 200 column (GE Healthcare) coupled to a Viscotek TDA tetra detector array (Malvern). The column was equilibrated with 50 mM Hepes pH 7.5, 100 mM NaCl and 0.023% DDM or 0.14% FC-12 at a flow rate of 0.3 $mL{\cdot}min^{-1}$ until a stable base line was attained (as measured by the absorbance at 280 nm). 100 µL of purified *Nm*EptA at a concentration of 1 $mg{\cdot}mL^{-1}$ was applied to the column. The data from the detectors (SEC-UV_{280}/right angle light scattering (LS)/refractive index (RI)) were analysed using the OmniSEC software.

Differential scanning fluorimetry. Differential scanning fluorimetry assays were performed using the thiol reactive flurorescent probe, 7 diethylamino-3-(4-maleimidophenyl)-4-methylcoumarin (CPM) (Santa Cruz Biotechnology Inc) in a CFX96 real-time PCR detection system with C1000 series thermocycler (Bio-Rad, USA). The protocol for the assay was adapted from Alexandrov *et al.* (7). The CPM dye was dissolved in dimethyl sulfoxide to a stock solution of 40 $mg{\cdot}mL^{-1}$. A working stock solution of the dye was prepared by diluting the stock to 2 $mg{\cdot}mL^{-1}$ with a buffer containing 50 mM Hepes pH 7.5. An aliquot of 0.4 µL of the CPM working stock was added to 1 µL of the protein purified

in DDM or FC-12, at approximately 20 mg·mL^{-1}. This mixture was further diluted to a final volume of 50 µL with the corresponding final purification buffer (containing either 3 x CMC concentrations of DDM or FC-12) and transferred immediately to the thermocycler. Assays were performed in duplicate. A temperature gradient of 25 to 75 ^{o}C in 1 ^{o}C intervals was used for the assay.

Circular dichroism spectropolarimetry (CD). Far-UV spectra were measured at 20 °C on a CD spectrophotometer (Jasco J-720) using a 1 mm path length quartz cuvette. The protein sample was diluted to a concentration of 0.4 mg·mL^{-1} in 20 mM sodium phosphate pH 7.0 with the different detergent (DDM, FC-12 and Cymal-6) at 3 X CMC and CD data collected every 1 nm with a 1 nm bandwidth in the 200 – 260 nm wavelength region using an integration time of 1 s per step. The resulting spectra represent the average of three accumulations and are buffer-baseline corrected and with the signal-to-noise ratio improved by Savitzky-Golay method (8) with the minimum convolution width (of 5 data points), using Spectra Analysis software (version 1.53.07 for Windows 95/NT, JASCO Corp.).

.

***Nm*EptA enzyme assay using NBD-PEA fluorescent lipid substrate**. Enzyme activity assays were performed using a substrate containing a fluorescent label, 1-acyl-2-{12-[(7-nitro-2-1,3-benzoxadiazol-4-yl)amino]dodecanoyl}-*sn*-glycero-3-phosphoethanolamine (Avanti Lipids) (NBD-PEA) to assess PEA transfer by the enzyme purified in different detergents. *Nm*EptA (1.2 mg·mL^{-1}) in buffers containing 50 mM Hepes pH 7.5, 100 mM NaCl and 3 X CMC of detergents (DDM, FC-12 and Cymal-6) was added to NBD-PEA (0.4 mM) and equilibrated at room temperature for 16 hours. The reactions were applied to a TLC plate and developed using ethyl acetate:methanol:water (7:2:1). The fluorescence signal on the plate was visualised in the Chemidoc MP imaging system (Bio-Rad) using Epi blue light (455-485 nm) and a corresponding filter (530 nm +/- 28 nm). For confirmation of product formation (1-acyl-2-{12-[(7-nitro-2-1,3-benzoxadiazol-4-yl)amino]dodecanoyl}-*sn*-glycerol) the appropriate material on the TLC plate was scraped off and washed with methanol. Concentration of the eluent gave a residue that was analysed using a Waters LCT premier spectrometer, run in

positive ion, W-mode, using the atmospheric pressure chemical ionization (APCI) method with MeCN/0.1% formic acid in H_2O (9:1) as a matrix. HR-MS (APCI) *m/z* 691.4654; $[M+H]^+$ requires 691.4646.

***Neisseria flavescens* strain 4322 and LOS extraction.** *N. flavescens* strain 4322 was available in the Center for Immunochemistry from the collection of the late Herman Schneider, formerly of the Walter Reed Army Institute of Research. LOS was extracted and purified by a modification of the hot phenol-water method (9, 10).

Reaction of *Nm*EptA with *N. flavescens* LOS. We previously showed that lipid A of *N. flavescens* LOS has two phosphates and no PEA substituents (11). Therefore, LOS of *N. flavescens* was used as an acceptor for reaction with *Nm*EptA. LOS from *N. flavescens* (2 mg·mL^{-1}) and the substrate PE from *E. coli* (2 mg·mL^{-1}; Sigma-Aldrich, St. Louis, MO) were suspended with *Nm*EptA (8 μg·mL^{-1}) in 300 μl of 50 mM Hepes buffer with 100 mM NaCl at pH 7. The reaction was incubated at 37 °C with end-over-end rotation and intermittent shaking for 24 h when it was stopped by freezing (-20 °C). The LOS was pelleted by centrifugation at 18,000 x *g* for 5 min after the reaction and the buffer removed. Next, the LOS was washed with water (300 μL) and centrifuged to remove salts twice.

MALDI-TOF mass spectrometry. Intact LOS samples were prepared for MS analysis using a previously described method. Briefly, washed LOS (10 mg·mL^{-1}) was suspended in a methanol-water (1:3) solution with 5 mM EDTA, and an aliquot was desalted with a few cation exchange beads (Dowex 50WX8-200) that had been converted to the ammonium form. The desalted sample solutions were mixed with 100 mM dibasic ammonium citrate (9:1, vol/vol), and then 1.0-2.0 μL were deposited on top of a dried, thin layer matrix that had been spotted within inscribed circles on the stainless steel sample plate. The matrix solution (deposited in 1.0 μL aliquots) was prepared from 2,4,6-trihydroxyacetophenone (200 mg·mL^{-1}; Sigma-Aldrich) in methanol and nitrocellulose transblot membrane (15 mg·mL^{-1}; Bio-Rad, Hercules, CA) in acetone-isopropanol (1:1, vol/vol), mixed in a 3:1

(vol/vol) ratio. MALDI spectra of the LOS were acquired on a linear-mode Microflex LT instrument (Bruker Daltonics Inc., Billerica, MA) equipped with a 337-nm N_2 laser operating at 30 to 60 Hz. The instrument was operated with FlexControl 3.3 software and run in the negative-ion mode at an acceleration voltage of 20 kV with pulsed ion extraction. Approximately 500 laser pulses were acquired per spectrum. The instrument was externally calibrated with the average masses for bovine insulin at m/z 5,732.58, insulin β-chain at m/z 3,494.94, renin substrate at m/z 1,758.06, and angiotensin II at m/z 1,045.20 (all from Sigma-Aldrich), and then a single-point internal correction was made to the spectra using the prompt fragment for diphosphorylated lipid A at m/z 1713.2. FlexAnalysis 3.3 software was used to digitally smooth and correct the baseline of the spectra.

TNFα response of human monocytes. The human monocytic leukemia cell line THP-1 (ATCC) was cultured in RPMI 1640 supplemented with 10 % fetal bovine serum (FBS) at 37°C in 5 % CO_2 and differentiated with 10 ng·mL^{-1} phorbol myristate acetate (Sigma-Aldrich) for 18 h. Differentiated cells were seeded in 96-well plates (10^4 cells per well) and treated for 18 h with *N. flavescens* LOS (100 ng·mL^{-1}) after incubation with or without *Nm*EptA, or with *Nm*EptA without any LOS. Cell culture supernatants were assayed for TNFα levels by enzyme-linked immunosorbent assay (ELISA) according to the instructions of the manufacturer (human TNFα ELISA Ready-SET-Go; eBioscience, San Diego, CA).

Quenching intrinsic fluorescence experiments. Intrinsic fluorescence was monitored using an EnSpire Multimode plate-reader (Perkin-Elmer). Samples were excited at 295 nm (100 flashes; <8 nm bandwidth), in order to selectively excite tryptophan, and emission spectra were measured in 1 nm intervals. For quenching experiments, spectra were recorded after addition of an aliquot (1, 2 or 3 µL) of stock salt solutions (4 M potassium iodide (KI), or potassium chloride (KCl)) to samples. The iodide stock solution contained 0.2 mM sodium thiosulphate to prevent the formation of triiodide (I_3^-) (12). The initial composition of the protein samples was: 100 µL of 24 µM *Nm*EptA (purified in DDM, Cymal-6 or FC-12), 50 mM Hepes, 50 mM NaCl, with 50 mM KCl or KI and detergent concentration at 3 x

CMC. For denatured protein experiments, β-mercaptoethanol (βME) was included in KCl and KI stocks to insure reducing conditions through-out the experiment, thus initial and final composition included 4.0 M guanidine, 2.0 mM βME, and 3.5 M guanidine, 25 mM βME, respectively. Samples were incubated (10-15 min at 20 ˚C) in an UV-Star® half-area microplate (Greiner Bio-One). Triplicate spectra were recorded for three replicate protein wells and three replicate protein-free wells of same volume and equivalent buffer and salt compositions, with the former buffer-baseline corrected by subtraction by the latter.

Data obtained from quenching experiments was fitted using equation 1, where [I] corresponds to iodide concentration, to determine the Stern-Volmer constant (K_{SV}):

$$F_0/F = K_{SV} \cdot [I] + 1 \qquad \text{[Equation 1 (12)]}$$

Relative fluorescence intensities (F_0/F) of unquenched protein fluorescence dividing by quenched protein fluorescence, were obtained by dividing protein fluorescence in presence of KCl by protein fluorescence by that obtained at the equivalent KI concentration. This corrects for changes to ionic strength and volume that occur with each addition of quenching, or non-quenching salt (*i.e.* KI and KCl, respectively). K_{SV} was determined using fluorescence emission recorded at 350 nm, as this corresponds to fluorescence from the surface-exposed tryptophan residues that will be most quenched by KI. Equation 1 was fitted to the linear regions of the quenching data using linear regression in GraphPad Prism software (version 5.02 for Windows, GraphPad Software Inc.).

Limited proteolysis. Limited proteolysis of *Nm*EptA purified in DDM micelles, FC-12 micelles and Cymal-6 micelles was performed with trypsin and chymotrypsin (both purchased from Sigma Aldrich) at 37^{o}C. Digestions were carried out at an *Nm*EptA concentration of 2.5 mg·mL^{-1} using *Nm*EptA to proteolytic enzyme ratio of 1:1000 by weight. The digestion was sampled over 24 hours (0, 0.25, 0.5, 1, 3, 6 and 24 hours) and the proteolysis of the sample was stopped by addition of 1mM PMSF. The digested samples were analysed by SDS-PAGE under reducing conditions and imaged by the

Chemidoc MP imaging system (Biorad). Further analysis of the proteolytic fragments of *Nm*EptA was performed by mass spectrometry in order to map the region of the proteolytic fragments corresponding to the *Nm*EptA structure. Bands from the SDS-PAGE gel for the 6 hour digested samples were excised. Matrix CHCA (α-Cyano-4-hydroxycinnamic acid) was prepared to a concentration of 1 $mg.mL^{-1}$ with 80% acetonitrile (ACN)/ 0.1% trifluoroacetic acid / 10 mM ammonium citrate. Dry peptide samples were reconstituted in (50:50 ACN:water) and spotted 1:1 with matrix onto a 384-well Opti-TOF stainless steel plate. MALDI-TOF/TOF spectra were acquired on a AB Sciex TOF/TOF 5800 mass spectrometer. The peptides identified by mass spectral analysis were compared and correlated to the theoretical mass and peptide sequence of tryptic and chymotryptic digested *Nm*EptA fragments generated by the online software: PeptideMass (13).

Molecular dynamics simulations. DPPE system setup. The *Nm*EptA crystal structure was taken as the starting conformation. To estimate the initial position of the TM domain in the lipid bilayer, a set of preliminary simulations with the TM domain placed at two different depths within DPPE bilayer were carried out in duplicate for 45 ns. The first placement had TM domain oriented with the longest helices oriented perpendicular to the membrane, which enables the TM domain to span the membrane, but the PH2 and PH2' helices and the bridging helix were buried in the bilayer. The second placement was done in a way that the bridging helix was placed parallel to and just slightly above the membrane surface. The latter placement proved to be a feasible one, an the final TM domain orientation was similar to that obtained by the *Orientations of Protein in Membrane* (OPM) server (http://opm.phar.umich.edu/server.php). The final conformation from the simulation run with the least deviation from the initial crystal structure (3.1 ± 0.3 Å) was taken as a starting point to rebuild the system containing the entire protein (including the soluble domain). The soluble domain was superimposed to the equilibrated TM domain, while preserving the crystallographic orientation as closely as possible, resulting with a slightly modified initial protein conformation compared to the original crystal structure with an approximate 3 Å RMSD between the two (SI Appendix, Fig. S8). In addition to the protein, the final system contained one Zn^{2+} ion in the *Nm*EptA active site, 832 DPPE

lipids, 85000 SPC water molecules. Three Na^+ ions were added to maintain the overall charge neutrality of the system. Prior to production runs, the system was energy minimized and equilibrated by gradually releasing the positional restraints over a 3 ns timeframe. A total of 6 independent simulations were carried out, 3 at 298 K and 3 at 310 K. All MD simulations were performed using GROMACS (14) version 3.3.3 in conjunction with the GROMOS 54A7 force field for proteins (15). Lipid parameters and equilibrated DPPE bilayer were derived by Piggot *et al*. (16) and obtained through the Lipidbook repository (17) The simple point charge (SPC) water model (18) was used to describe the solvent water.

PE/PG system setup. A mixed bilayer containing 80% 1-palmitoyl-2-palmitoleyl-*sn*-glycero-3-phosphoethanolamine (PPoPE) and 20% 1,2-dimyristoyl-sn-glycero-3-phospho-(1'-rac)-glycerol (DMPG) was constructed starting from the equilibrated 1-palmitoyl-2-oleyl-*sn*-glycero-3-phosphoethanolamine (POPE) bilayer. Please note that this bilayer contains both L and D-enantiomer of DMPG head group, while only L-enantiomer (sn-glycero-1-phosphate) occurs naturally in biological membranes. The DMPG and POPE force field parameters and the initial equilibrated POPE bilayer were taken from Piggot *et al.* (16), which were made available on the Lipidbook repository. The initial POPE lipid parameters were modified to PPoPE lipid by removing the last two carbon atoms of the oleic fatty acid tail (C18:1, ω-9 unsaturated fatty acid) to obtain palmitoleic acid found in the Neisserial bacterial membrane (C16:1, ω-7 unsaturated fatty acid). This particular composition was chosen based on the results of mass-spectrometry characterization of the Neisserial phospholipid composition. This study revealed that the most common phospholipid head group in the several different strains is phosphatidylethanolamine (PE, 65-77%), followed by phosphatidylglycerol (PG, 14-20%) and phosphatidic acid (PA, 8-11%). Fatty acid composition analysis showed a large proportion of short-chain fatty acyl substituents (C12:0, C14:0, C14:1) in the Neisserial phospholipids in comparison to other Gram-negative enteric bacteria. Thus, myristic fatty acids were used in combination with PG head groups. The similarity in the ratio of highly represented C16:1 and C16:0 fatty acids (33% and 30%, respectively) provided a motivation for their use in combination with PE

head groups, to give PPoPE lipids. The mixed PE/PG bilayer was further equilibrated at 298 K for 40 ns prior to incorporation of the protein.

As the DPPE simulations showed that positioning the bridging helix just above the membrane provides a reasonable starting point for membrane insertion, the initial equilibration of the isolated TM domain was omitted in the construction of *Nm*EptA -PE/PG system. Instead, this orientation was applied to the entire *Nm*EptA protein, including the soluble domain, to initiate simulations of *Nm*EptA in the PE/PG membrane. The final system contained one Zn^{2+} ion in the *Nm*EptA active site, 386 PPoPE lipids, 100 DMPG lipids, 50000 SPC water molecules, 0.1 M concentration of NaCl and additional ions to neutralize the system, resulting with the addition of total 240 Na^{+} and 135 Cl^{-} ions. Here the system was energy minimized and equilibrated by gradually releasing the positional restraints over a 5 ns timeframe, followed by three independent production runs at 298 K. Simulations were carried out using the GROMACS 3.3.3. engine and GROMOS 54A7 force field.

Simulation parameters. Each simulation was performed in a rectangular box, under periodic boundary conditions. The dimensions of the box were chosen so that the minimum distance between any atom of the protein and the box wall was at least 1.0 nm. A twin-range method was used to evaluate the non-bonded interactions. Interactions within the short-range cutoff of 0.8 nm were updated every step. Interactions within the long-range cutoff of 1.4 nm were updated every 2 steps, together with the pair list. A reaction field correction was applied using a relative dielectric constant of ε_r = 78.5 to minimize the effect of truncating the electrostatic interactions beyond the 1.4 nm long-range cut-off (19). The LINCS algorithm (20) was used to constrain the lengths of the covalent bonds. The geometry of the water molecules was constrained using the SETTLE algorithm (21). The simulations were carried out in the NPT ensemble at T = 300 K and P = 1 bar. The temperature and pressure were maintained close to the reference values by weakly coupling the system to an external temperature (22) and pressure bath using a relaxation time constant of 0.1 ps and 0.5 ps, respectively. The pressure coupling was semi-isotropic. The integration timestep used was 2 fs. Data was collected for analysis every 50 ps. Root mean squared deviation (RMSD) of the backbone atoms of the entire

protein and each domain separately was calculated after the least square fit alignment of the frames with respect to the initial conformation for the relevant atom selection. Images were produced using VMD (23).

Supporting Simulation Results. Despite the short length of the TM domain in comparison to the membrane thickness, the TM domain is able to span both the DPPE and PE/PG bilayer, maintaining its position and orientation within the membrane in all simulations. The length of the positively charged side-chains of Lys142, Lys144, Arg146 and Lys150 at the cytoplasmic end of TMH5 provides the additional length needed for the TM domain to fully span the bilayer (Supporting Movie S1 and S2), anchoring the soluble domain.

The secondary structure and overall fold of both domains remained stable throughout all MD simulations. The backbone RMSD of the TM and soluble domain ranged between 2 -3 Å across the 6 simulations, while for the simulations resulting with the "open" conformation increased RMSD to 4-5 Å for each domain. In both domains, fluctuations in loop regions are the main contributors to the observed RMSD, while the major structural features of the nine final conformations from each simulation show a high degree of structural overlap (SI Appendix, Fig. S8B, C). In the soluble domain, these disordered loops are often involved in the interactions with lipid head groups, especially in the "open" conformation of the soluble domain. The molecular interactions triggering the conformational change remain unclear, however the positively charged residues dispersed on the surface of the soluble domain play an important role in the steering and binding of the soluble domain to the membrane surface (SI Appendix, Movie S1 and S2).

The conformational change from the MD simulation exposes a large charged electrostatic surface at the interface of the membrane and soluble domains (SI Appendix, Fig. S9). In the more "open" conformations the charged patch on the soluble domain, is orientated away from the lipid bilayer. In the more "closed" conformation, such as that observed in the full-length *Nm*EptA structure, the active site nucleophile is more sequestered in a conformation which is potentially relevant for catalysis. Despite the differences between the simulation conditions, there is a consistent picture of

conformational space sampled by *Nm*EptA in the lipid bilayer: the soluble domain interacts with the membrane surface and it is able to adopt a range of orientations with respect to the TM domain (SI Appendix, Fig. S9). As a result of these interactions with the soluble domain, the curvature of the bilayer changes, regardless of the composition of bilayer used in the simulations.

Determining sequences for inclusion in alignment. The sequence alignment in SI Appendix, Fig. S1 includes only PEA transferases that can transfer PEA to the 4' and/or 1 phosphates of Lipid A. The genome of *Nm* contains 4 genes encoding PEA transferases, however, only the gene product of *eptA* modifies these phosphates within the head group of Lipid A, and this Lipid A modification in *Nm* causes resistance to polymyxin. PEA transferase which act on the same region of Lipid A as *Nm*EptA were determined based on evidence in the literature. In bacterial species where a single homologue of EptA was reported (*e.g. ept*C in *Campylobacter jejuni* (24) and *pmr*C in *Acinetobacter baumannii* (25)), EptA enzymes were identified by their reported ability, indicated by mass spectra, to modify Lipid A and the correlation of increased / decreased protein expression level with increased / decreased bacterial resistance to polymyxin (24, 25). In the case of *C. jejuni*, the EptA annotated as *ept*C, modifies a wide range of substrates, including the head region of Lipid A (in analogous manner to *Nm*EptA), the inner core oligosaccharide of LOS, and various proteins (24, 26). In *Haemophilus ducreyi*, three PEA transferases were identified by sequence homology, but the only the gene product of HD0852 was shown by mass spectrometry to modify Lipid A (27). In *Salmonella enterica* serovar Typhimurium, two PEA transferases have been identified and are annotated as *pmr*C/STM4293 and *cpt*A/yijP/STM4118 (28). Proton NMR spectra of LPS extracted from two *S. enterica* gene-knockout strains indicate that *cpt*A acts on the inner core oligosaccharide of LOS (28) whereas mass spectra show that the *pmr*C acts on Lipid A in analogous manner to *Nm*EptA (29). In *E. coli*, six PEA transferases have been identified by sequence homology (30), and are referred to as the YhbX/YhjW/YijP/YjdB family (31). TLC analysis of Lipid A from different *E. coli* strains over-expressing each putative PEA transferase has indicated that only the gene product of *ept*A (also annotated as *yjd*B/*pmr*C) modifies a phosphate in the Lipid A head group (31).

Table S1: Data collection and refinement statistics.

Crystal Statistics	
Space Group	I422
Unit Cell Dimensions	a = 187.29 Å b = 187.29 Å, c = 205.13 Å, α = 90°, β = 90°, γ = 90°
Data Processing Statistics	
Resolution (Å)	46.82 - 2.75 (2.85 - 2.75)
Total reflections	94785 (9347)
Unique reflections	47424 (4674)
Multiplicity	2.0 (2.0)
Completeness (%)	99.96 (100.00)
Mean I/σ(I)	9.26 (1.20)
R-merge	0.076 (0.72)
R-measured	0.1072
$CC_{1/2}$	0.993 (0.527)
Data Refinement Statistics	
R-work	0.214 (0.307)
R-free	0.241 (0.352)
Number of non-hydrogen atoms	4435
Protein atoms	4253
Ligand atoms	56
Water molecules	126
RMS bonds (Å)	0.011
RMS angles (°)	1.05
Ramachandran favored (%)	94.8
Ramachandran outliers (%)	0.75
Average B-factor (Å^2)	46.6

Table S2: MALDI-TOF/TOF analysis of limited proteolysis

Molecular Weight (kDa)[3]	Peptide sequence identified by MALDI -TOF/TOF				Predicted cleavage sites[1,2]
Trypsin Digest					
	***Nm*EptA in DDM[1]**	**Structural Region[2]**	***Nm*EptA in FC-12[1]**	**Structural Region[2]**	**1** MIKPNLRPK **9(MD)** **10** LGSSALIAFLSLYSSLVLNYAFFAK **34(MD)** **35** VVELHPFNGTGADIFLYTMPVVLFFLSNFVFHVIALPFV HK **75 (MD)** **76** VLIPLILVISAAVSYQEIFFNIYFNK **101(MD)** **102** SMLNNVLQTTAAESAR **107(MD)** **108** LITPGYVLWIVCLGVLPALAYIAVK **142(MD)** **147** VWYKEFLTR **155(MD)** **156** LVLAAVSFLCALGIAMLQYQDYASFFR **182(MD)** **186** SVTHLIVPSNFIGAGVSK **203 (PH4, BH)** **210** SNIPYTQLDMAVVQNRPAGSLR **231 (SD)** **232** RFVVLVVGETTR **243(SD)** **244** AANWGLNGYSR **254 (SD)** **255** QTTPLLAAR **263 (SD)** **264** GDEIVNFPQVR **274 (SD)** **275** SCGTSTAHSLPCMFSTFDR **293 (SD)** **294** TDYDEIK **300 (SD)** **301**AEHQDNLLDIVQR **313 (SD)** **314** AGVEVTWLENDSGCKGVCGK **333 (SD)** **334** VPNTDVTSLNLPEYCR **349 (SD)** **350** NGECLDNILLTK **361 (SD)** **362** FDEVLNKNDKDAVLILHTIGSHGPTYYER **390 (SD)** **391** YTEAERK **397 (SD)** **398** FTPTCDTNEINK **409 (SD)** **413** ATLVNTYDNTVLYVDQFIDKVIRKLENR **440 (SD)** **441** DDLESVVHYVSDHGESLGENGMYLHAAPYAIAPSGQTHIP
60	**103** SMLNNVLQTTAAESAR **117**	**(MD)**			
	187 SVTHLIVPSNFIGAG **200**	**(PH4, BH)**			
	210 SNIPYTQLDMAVVQNR PAGSLR **231**	**(SD)**			
	233 FVVLVVGETTR **243**	**(SD)**			
	244 AANWGLDGYSR **254**	**(SD)**			
	255 QTTPLLAAR **264**	**(SD)**			
	265 GDEIVNFPQVR **276**	**(SD)**			
	194 TDYDEIKAEHQDNLL DIVQR **313**	**(SD)**			
	371 DAVLILHTIGSHGPTY YER **390**	**(SD)**			
	413 ATLVNTYDNTVLYVDQF IDKVIR **435**	**(SD)**			
42	**233** FVVLVVGETTR **243**	**(SD)**	**187** SVTHLIVPSNFIGAGVSK **203**	**(PH4, BH)**	
	244 AANWGLDGYSR **254**	**(SD)**	**233** FVVLVVGETTR **243**	**(SD)**	
	255 QTTPLLAAR **264**	**(SD)**	**255** QTTPLLAAR **264**	**(SD)**	
	265 GDEIVNFPQVR **276**	**(SD)**	**265** GDEIVNFPQVR **276**	**(SD)**	
	194 TDYDEIKAEHQDNLLD IVQR **313**	**(SD)**	**194** TDYDEIKAEHQDNLLDIVQR **313**	**(SD)**	
	371 DAVLILHTIGSHGPTY YER **390**	**(SD)**	**371** DAVLILHTIGSHGPTYYER **390**	**(SD)**	
	413 ATLVNTYDNTVLYVDQ FIDKVIR **435**	**(SD)**	**413** ATLVNTYDNTVLYVDQF IDKVIR **435**	**(SD)**	
30	**187** SVTHLIVPSNFIGAG **200**	**(PH4, BH)**			
	233 FVVLVVGETTR **243**	**(SD)**			
	255 QTTPLLAAR **264**	**(SD)**			
26	**187** SVTHLIVPSNFIGAG **200**	**(PH4, BH)**			
23			**233** FVVLVVGETTR **243**	**(SD)**	
			255 QTTPLLAAR **264**	**(SD)**	

					MVMWFSK **487 (SD)** **491** QHGGIDFQCLK **501(SD)** **504** AAENEYSHDHYFSTVLGLMDISNSQTYRKEMDI LAAC **541(SD)** **542** RPRKASHHHHHH **553 (SD)**
Chymotrypsin Digest					
	***Nm*EptA in DDM** [1]	**Structural Region**[2]	***Nm*EptA in FC-12**[1]	**Structural Region**[2]	
42	**233** FVVLVVGETTR **243**	**(SD)**	**187** SVTHLIVPSNFIGAG **200**	**(PH4, BH)**	**1** MIKPNLRPKLGSSALIAFLSLY **22 (MD)** **23** SSLVLNY **29 (MD)** **33** AKVVELHPFNGTGADIFLY **51 (MD)** **52** TMPVVLFFLSNFVFHVIALPFVHKVLIPLILVISAAVSYQEIFF NIYFNKSMLNNVLQTTAAESARLITPGYVLW **126 (MD)** **127** IVCLGVLPALAYIAVKVKY **145 (MD)** **150** KEFLTRLVLAAVSFLCALGIAMLQYQDY **177 (MD)** **178** ASFFRNNKSVTHLIVPSNFIGAGVSKY **204 (PH3, PH4, BH)** **215** TQLDMAVVQNRPAGSLRRFVVLVVGETTRAANWGLNGY **252** **253** SRQTTPLLAARGDEIVNFPQVRSCGTSTAHSLPCMFSTFD RTDYDEIKAEHQDNLLDIVQRAGVEVTWLENDSGCKGVCGKVPNTD KDAVLILHTIGSHGPTYYERY **391(SD)** **392** TEAERKFTPTCDTNEINKCTRATLVNTYDNTVLYVDQFIDK VIRKLENRDDLESVVHYVSDHGESLGENGMYLHAAPY 469 **(SD)** **470** AIAPSGQTHIPMVMWFSKAFRQHGGIDFQCLKQKAAEN EY **509 (SD)** **510** SHDHYFSTVLGLMDISNSQTY **530 (SD)** **531** RKEMDILAACRRPRKASHHHHHH **553 (SD)**
	255 QTTPLLAAR **264**	**(SD)**	**244** AANWGLDGYSR **254**	**(SD)**	
	265 GDEIVNFPQVR **276**	**(SD)**	**265** GDEIVNFPQVR 276	**(SD)**	
	194 TDYDEIKAEHQDNLL DIVQR **313**	**(SD)**	**194** TDYDEIKAEHQDNLLDIVQR **313**	**(SD)**	
	371 DAVLILHTIGSHGPTY YER **390**	**(SD)**	**371** DAVLILHTIGSHGPTYYER 390	**(SD)**	
	413 ATLVNTYDNTVLYVD QFIDKVIR **435**	**(SD)**	**413** ATLVNTYDNTVLYVDQFIDK **435**	**(SD)**	
34	**233** FVVLVVGETTR **243**	**(SD)**			
	244 AANWGLDGYSR **254**	**(SD)**			
	255 QTTPLLAAR **264**	**(SD)**			

	265 GDEIVNFPQVR **276**	**(SD)**			
	194 TDYDEIKAEHQDNL LDIVQR **313**	**(SD)**			
	371 DAVLILHTIGSHGPT YYER **390**	**(SD)**			
	413 ATLVNTYDNTVLYVDQ FIDKVIR **435**	**(SD)**			
25	**187** SVTHLIVPSNFIGAG **200**	**(PH4, BH)**			
	233 FVVLVVGETTR **243**	**(SD)**			
	255 QTTPLLAAR 264	**(SD)**			
20			**103** SMLNNVLQTTAAESAR **117**	**(MD)**	
			233 FVVLVVGETTR **243**	**(SD)**	
			255 QTTPLLAAR **264**	**(SD)**	
			371 DAVLILHTIGSHGPTYYER **390**	**(SD)**	

[1] The numbers correspond to the first and last residue of the peptide fragment obtained from proteolytic cleavage from the full length *Nm*EptA sequence.
[2] SD – soluble domain, MD – membrane domain, PH4 – periplasmic helix 4, BH – bridging helix.
[3] The font color corresponds to the color of the box around each molecular weight fragment band in SI Appendix, Fig. S6.

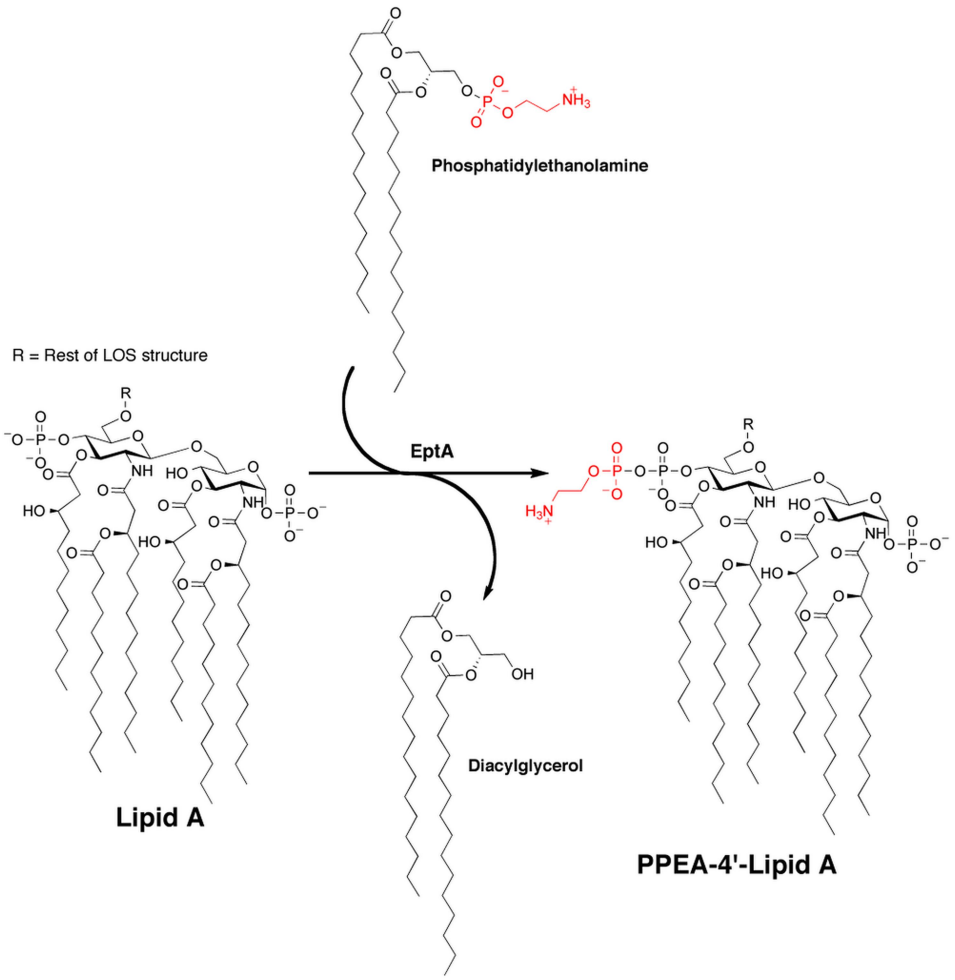

Scheme S1: Reaction catalyzed by EptA.

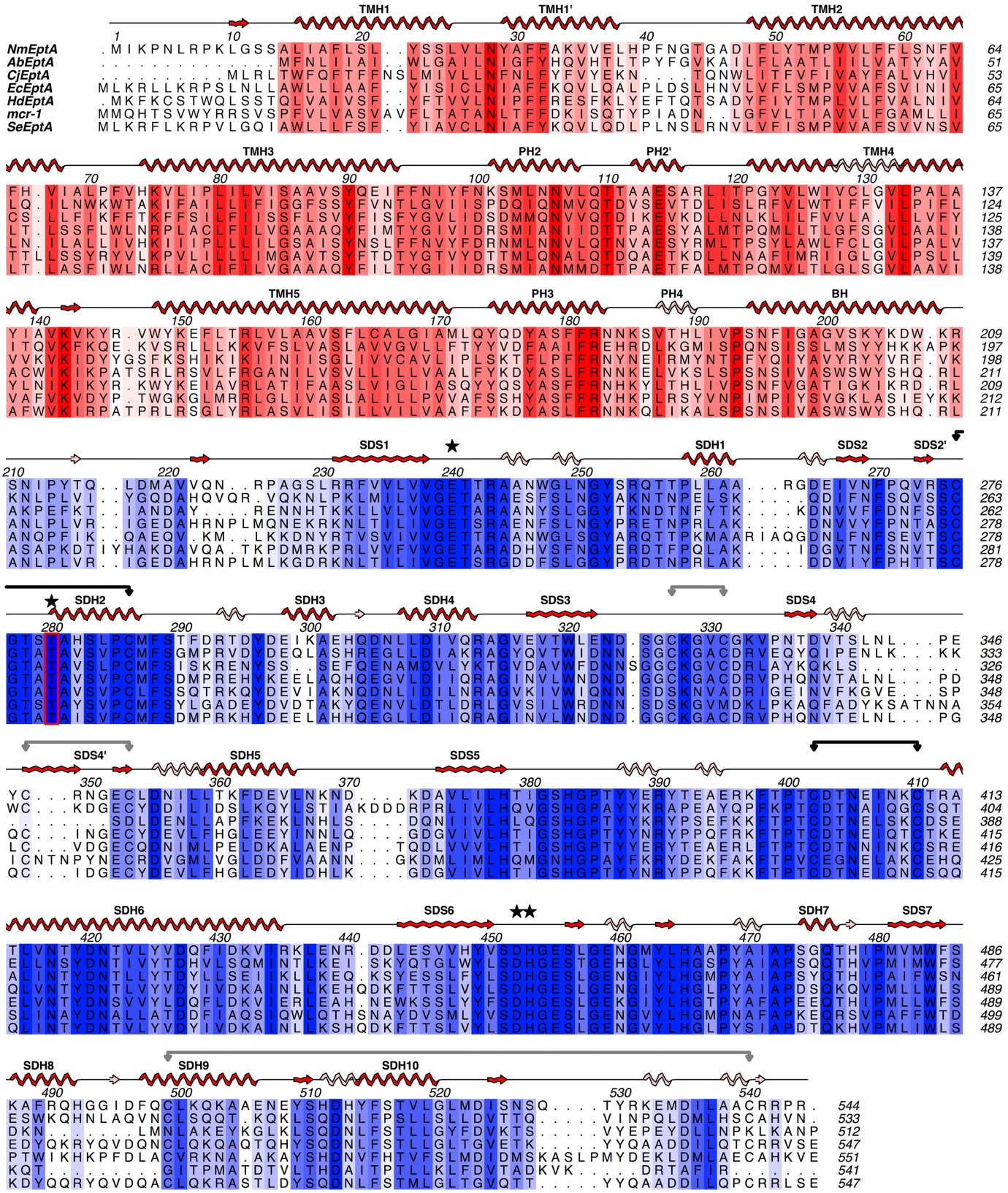

Fig S1. Multiple sequence alignment of PEA transferases. The alignment includes PEA transferases that transfer PEA to the 4' and 1 phosphates of Lipid A and was performed using CLUSTAL OMEGA (32). The secondary structure of *Nm*EptA (full length, PDB code 5FGN) is above the sequences, with α-helices and β-sheets in red and π-helices, 3_{10}-helices and β-bridges in pale pink, and was obtained using DSSP version 2.2.1 (33), which are annotated as in the topology diagram (Fig. 1B). The sequence

is shaded for physico-chemical similarity, in red for the TM domain and in blue for the soluble domain. Similarity analysis was performed in ALINE (34) and reflects the amino acid property groupings outlined in Livingstone and Barton, 1993 (35). The disulfide bonds observed in *Nm*EptA (both full-length, PDB code 5FGN and soluble domain structures, PDB codes 4KAV and 4KAY (36)) are shown with down-arrows (in black or gray corresponding to conserved or semi-conserved cysteines, respectively). A red box highlights the catalytic nucleophilic residue that is nonvariant in all PEA transferases. The residues involved in coordinating the bound Zn^{2+} ion in the full-length *Nm*EptA structure are marked with stars. Other EptA enzymes were identified as described in the methods. EptA is encoded by the gene *pmr*C in *Acinetobacter baumannii* (*Ab;* (25)), *pmr*C in *Salmonella enterica* (*Se*; (29)) and HD0852 in *Haemophilus ducreyi* (*Hd*; (27)), *ept*A in *E. coli* (*Ec*; (37)) and *ept*C in *Campylobacter jejuni* (*Cj*; (24)). The alignment also includes a recently identified PEA transferase (mcr-1) that causes plasmid-mediated polymyxin antibiotic resistance in Enterobacteriaceace such as *E. coli* (38).

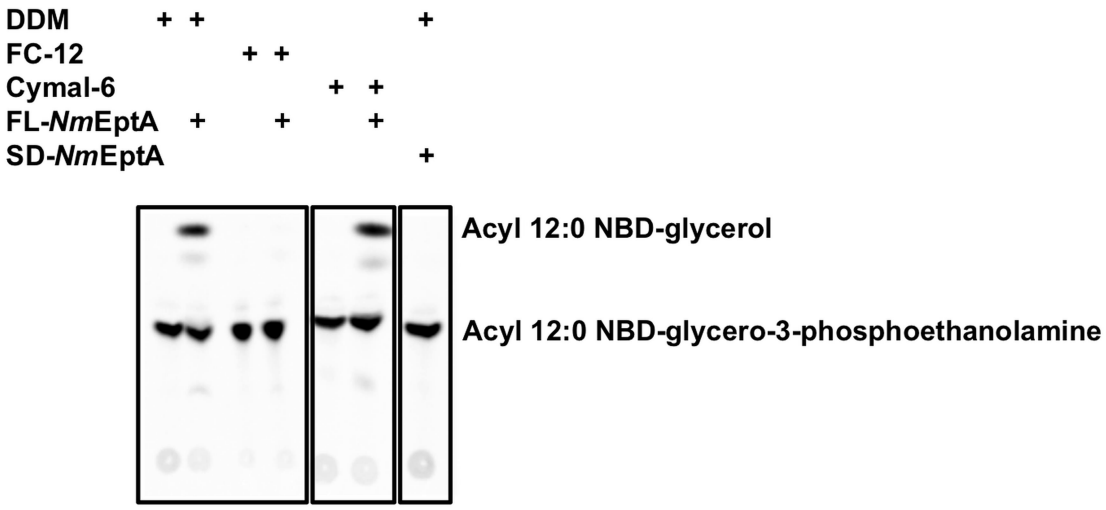

Fig. S2. Enzyme assay of recombinant *Nm*EptA purified in different detergent micelles. Thin layer chromatography assay using the fluorescent lipid substrate NBD-PEA on full length *Nm*EptA (FL-*Nm*EptA) solubilized and purified in different detergents (DDM, FC-12 and Cymal-6) and the soluble domain only (SD- *Nm*EptA). The substrate is labeled acyl 12:0 NBD-glycerol-3-phosphoethanolamine and the product is labeled acyl 12:0 NBD-glycerol.

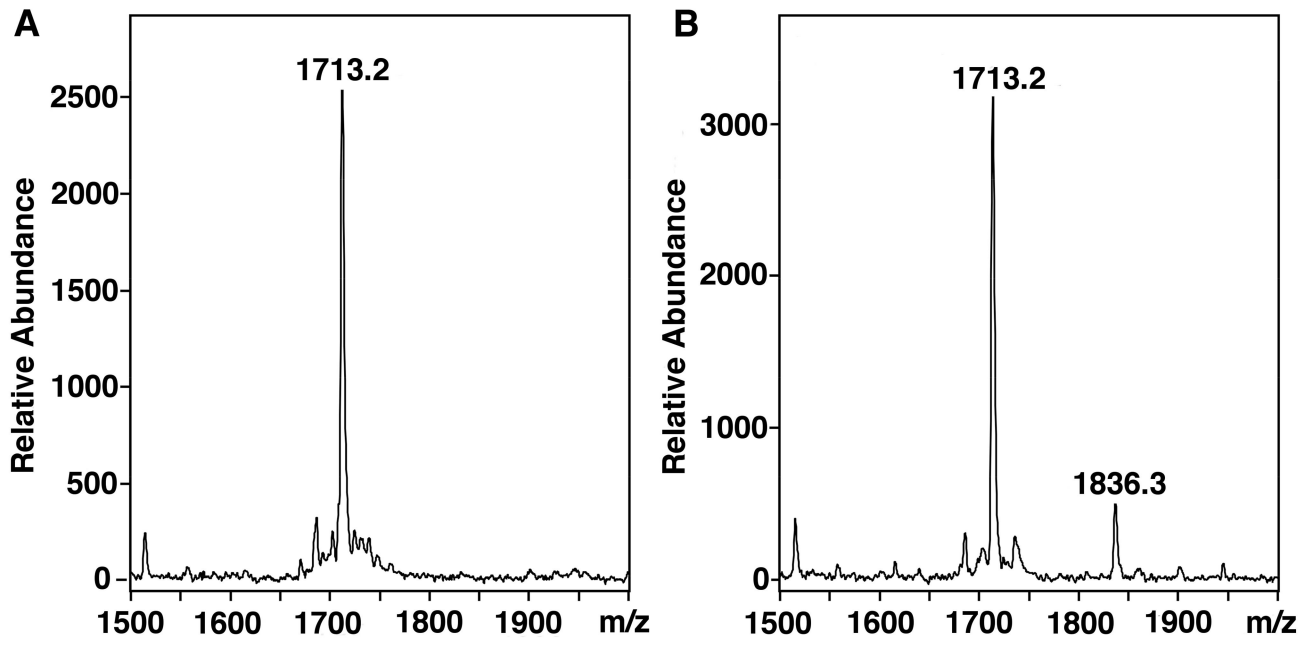

Fig. S3. MALDI-TOF mass spectrometry revealed recombinant *Nm*EptA catalyzed reaction of PE with Neisserial Lipid A. (A) Portion of the negative-ion MALDI-TOF mass spectrum of intact *N. flavescens* strain 4322 LOS. The Lipid A has two phosphate (P) moieties consistent with the prominent peak at m/z 1713.2 for prompt fragment ions of the conserved Neisserial lipid A. (B) Same region of the spectrum of *N. flavescens* LOS that had been treated with *Nm*EptA (8 μg·mL^{-1}) in the presence of the substrate PE (2 mg·mL^{-1}) for 24 h. A peak observed at m/z 1836.3 in the *Nm*EptA -treated LOS is consistent with the addition of a single PEA group (123 Da) to ions represented by the prominent peak at m/z 1713.2 for diphosphorylated Lipid A.

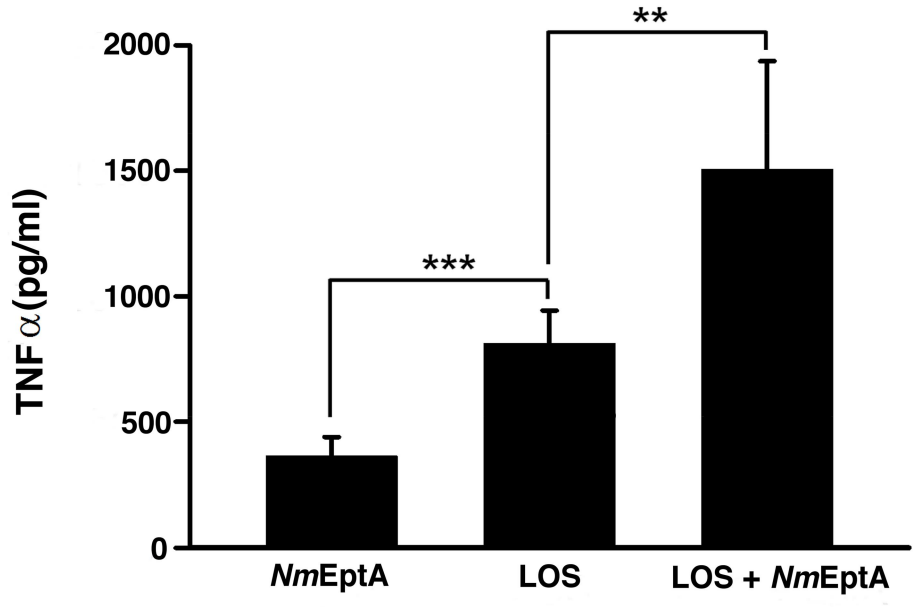

Fig. S4. ELISA shows addition of PEA group to LOS from *N. flavescens* increases the induction of TNFα in human THP-1 cells. ELISA was used to quantify TNFα levels in supernatants from human THP-1 cells that were incubated for 18 h with LOS (100 ng·mL^{-1}) from the commensal *N. flavescens* with or without pretreatment with *Nm*EptA, or with *Nm*EptA without any LOS. Data are representative of three independent experiments. The addition of PEA to the lipid A of *N. flavescens* LOS significantly increased TNFα induction compared to the induction by native untreated diphosphoryl LOS. *Nm*EptA alone induced significantly less TNFα compared to the unmodified LOS. (Error bars = SD; **p<0.01, ***p<0.001).

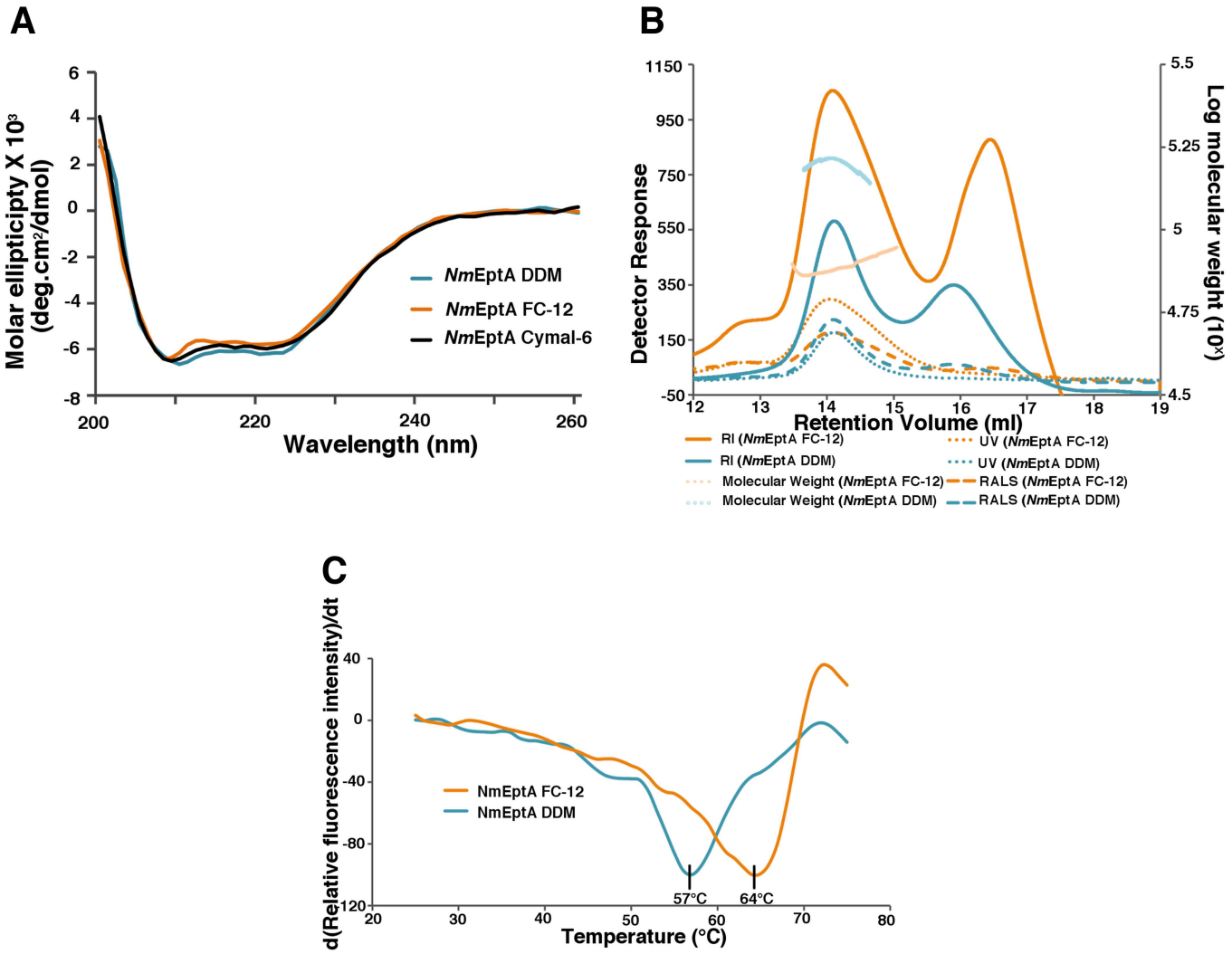

Fig S5. Biophysical analysis of *Nm*EptA solubilized and purified in the different detergents. (A) Comparison of CD spectra for *Nm*EptA in DDM, FC-12 and Cymal-6. (B) Comparison of SEC MALS profile for *Nm*EptA purified in DDM andFC-12. (C) A plot of the change in the relative fluorescence intensity with respect to time for *Nm*EptA in DDM and FC-12 using CPM. The negative of the 1st derivative was used to determine the melt temperature of the protein in DDM and FC-12 and normalised for comparison. The melt temperatures are indicated next to the corresponding curve.

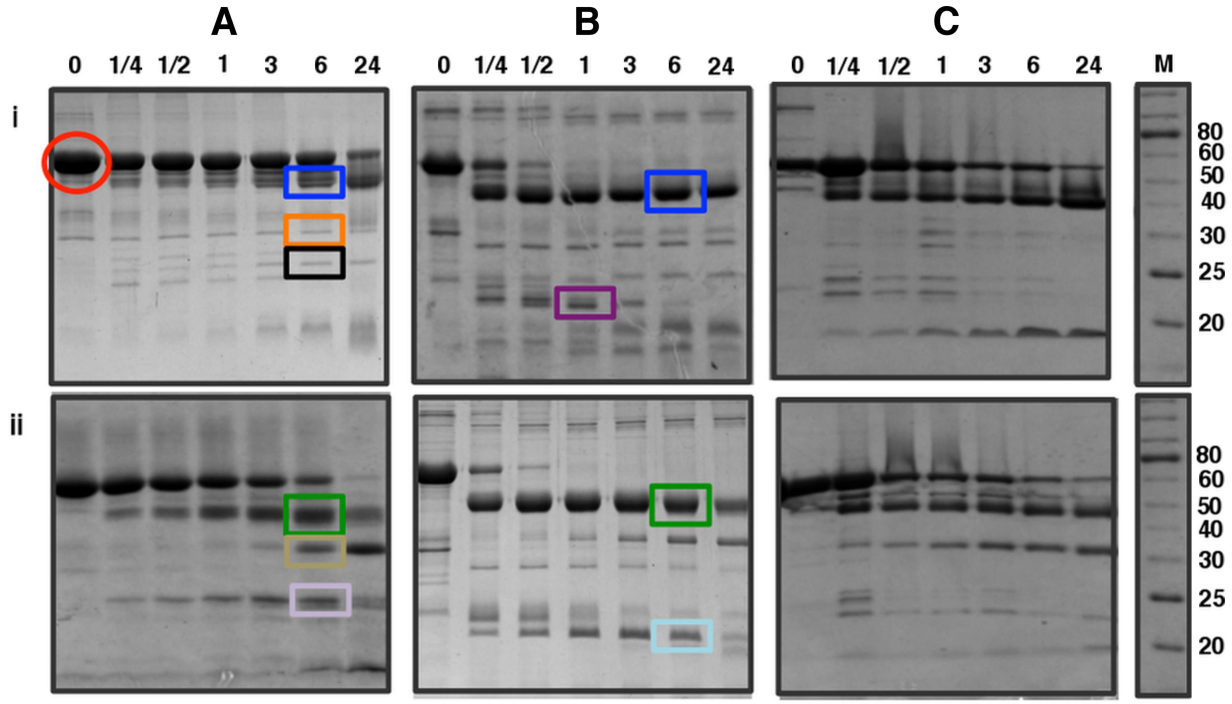

Fig. S6. SDS-PAGE analysis of limited proteolysis of *Nm*EptA. Limited proteolysis of *Nm*EptA solubilized in (A) DDM micelles, (B) FC-12 micelles, (C) Cymal-6 micelles. Panel *i* represents the profile after treatment of the enzyme with trypsin and panel *ii* represents the profile after treatment with chymotrypsin. The lanes on the gel represent the times of incubation with each of the proteases in hours. The bands indicated by a circle and rectangles were analysed by mass spectrometry. The peptide fragments identified for each coloured band correspond to the font colouring in SI Appendix, Table S2. The lane marked M represent the molecular weight markers as labelled in kilodaltons.

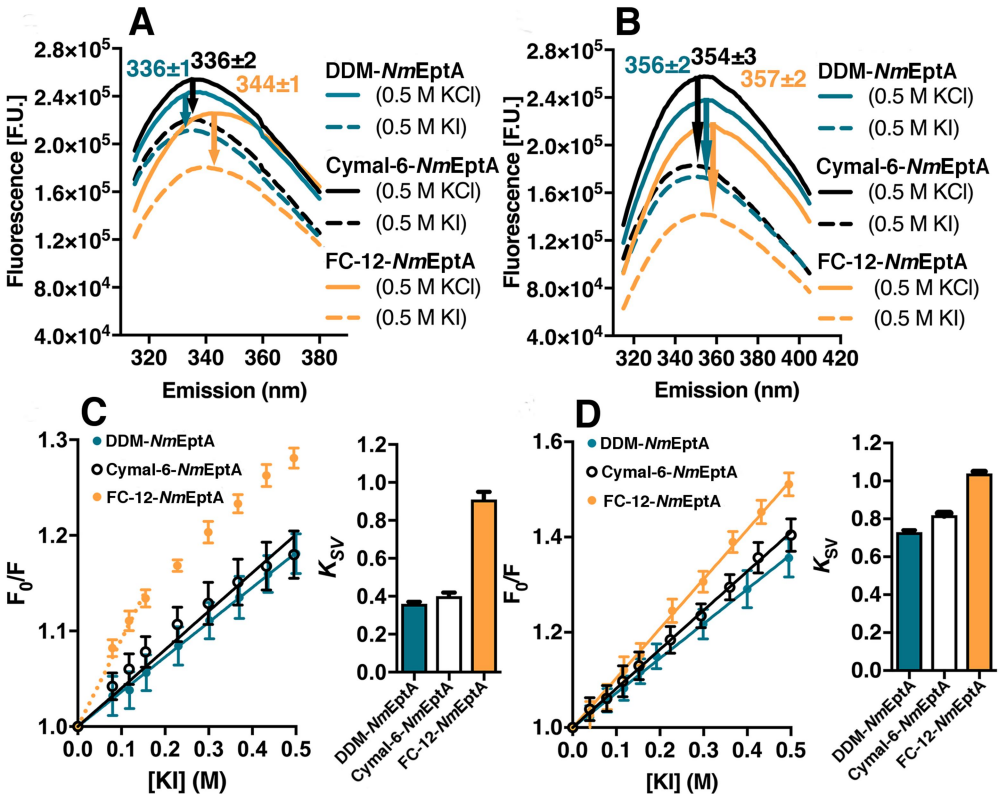

Fig. S7. Quenching profiles of the intrinsic fluorescence of *Nm*EptA. Emission spectrum of *Nm*EptA after excitation at 295 nm, for (A) non-denatured *Nm*EptA prepared in DDM, Cymal-6 or FC-12 and in (B) denatured *Nm*EptA prepared in DDM, Cymal-6 or FC-12. Each experiment was carried out in the presence of either 0.5 M KCl or 0.5 M KI (fluorescence quencher). The length of the arrows indicate the extent of quenching observed. Stern-Volmer plots and constants for (C) non-denatured *Nm*EptA and (D) denatured *Nm*EptA, quenched by iodide, reported at emission wavelength of 350 nm. Relative fluorescence intensities (F_0/F) of *Nm*EptA purified in DDM (blue symbols), Cymal-6 (open symbols) and in FC-12 (orange symbols) were fitted by linear regression to determine K_{SV} values (bars) for non-denatured DDM *Nm*EptA of 0.36 ± 0.01 M^{-1}, Cymal-6 *Nm*EptA of 0.40 ± 0.02 M^{-1}, and FC-12 *Nm*EptA of 0.91 ± 0.04 M^{-1}, and for denatured DDM *Nm*EptA of 0.73 ± 0.01 M^{-1}, Cymal-6 *Nm*EptA of 0.82 ± 0.01 M^{-1}, and FC-12 *Nm*EptA 1.04 ± 0.01 M^{-1}. The initial slope of the line (----) was used when curvature in the plots was observed. The error bars show the standard deviation of values determined in triplicate. In panel C the curvature for FC-12 *Nm*EptA indicates the tryptophans being quenched over iodide concentration range are differently surface exposed, which is further supported by the absence of the curvature in the denatured FC-12 denatured *Nm*EptA.

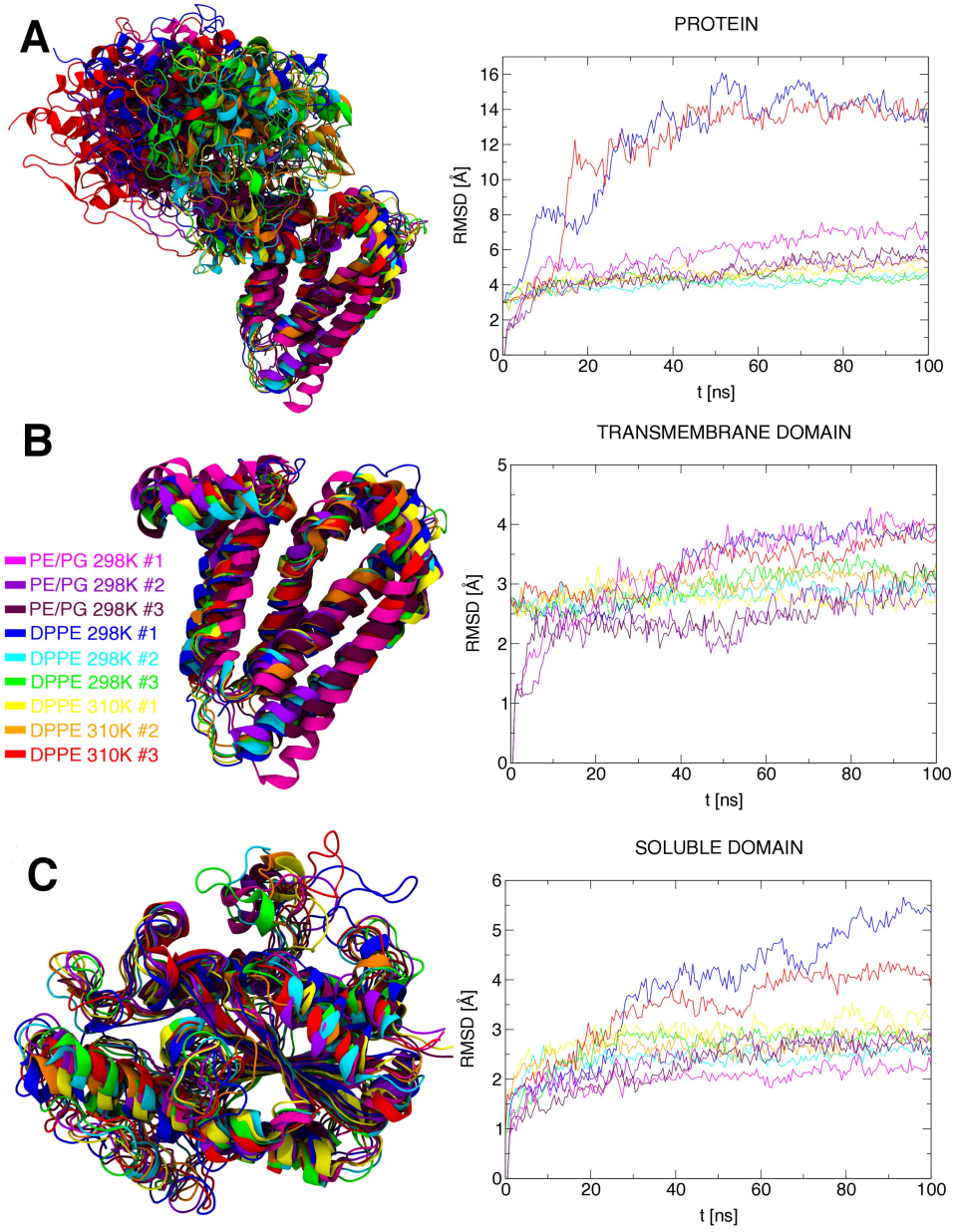

Fig. S8. Molecular dynamics results. RMS deviations and superposition of the relevant domains of the nine final *Nm*EptA conformations after 100 ns of simulation, obtained from nine independent simulations. Six of these *Nm*EptA simulations were in a DPPE bilayer at 298 K and 310 K, and three simulations were of *Nm*EptA embedded in the mixed PE/PG bilayer at 298 K. The simulations are colored according to the legend. (A) RMS deviations of the entire protein backbone during the simulations with respect to the initial crystal structure The alignment of the overlapped protein structures shown was based on TM residues only to illustrate mobility of the soluble domain, however the entire backbone was used for structural alignment prior to RMSD calculations. (B) and (C) RMS deviations of the (B) TM and (C) soluble domain from the initial crystal structure starting point

positioned in the membrane, respectively. The residues included in the analysis of TM domain ranged from Gly11 – Ala185, while the soluble domain was defined with residues Arg232 – Arg544. The RMSD values were shown for snapshots taken every 500 ps for clarity, due to the significant overlap of points sampled with higher frequency. The difference in RMSD at t=0 ns between the simulations in DPPE and PE/PG bilayer reflects slightly different starting *Nm*EptA conformations due to the pre-equilibration of TM domain in DPPE bilayer (SI Appendix, Materials and Methods).

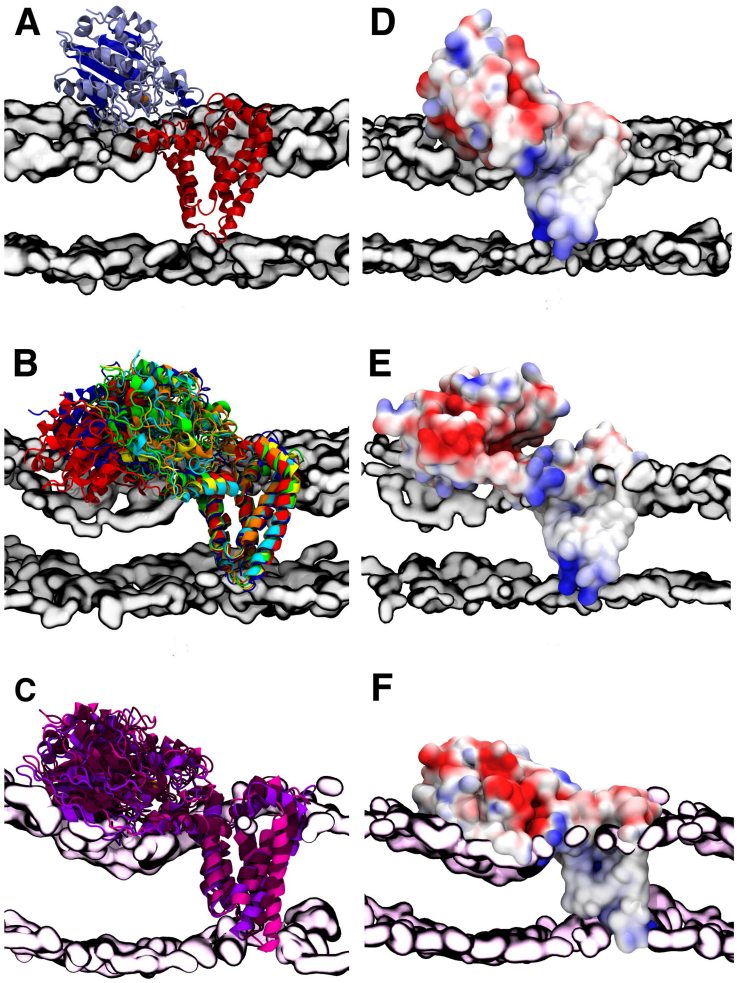

Fig. S9. Molecular dynamics simulations of *Nm*EptA in a DPPE membrane environment. (A) Initial snapshot of the equilibrated *Nm*EptA structure embedded in the DPPE bilayer with Zn^{2+} ion is shown as an violet sphere and silver surface representation of the lipid polar heads. (B) Superposition of the 6 *Nm*EptA conformations obtained after 100 ns at 298 K and 310K in DPPE bilayer. (C) Superposition of the 3 *Nm*EptA conformations obtained after 100 ns at 298 K in a mixed PE/PG bilayer, depicted as a pale pink surface representation of the lipid polar heads. Electrostatic surface representation of (D) the closed (298 K) and (E) open conformations of *Nm*EptA (298 K) observed in DPPE bilayer, and (F) the *Nm*EptA conformation obtained in the mixed PE/PG bilayer after 100 ns. The red colored regions on the electrostatic surface represent negatively charged surfaces (-3 kT/e) and the blue regions represent positively charged surfaces (+3 kT/e). The partial charges and atomic radii used for computing the electrostatic surface with APBS were taken from the Gromos54a7 force field.

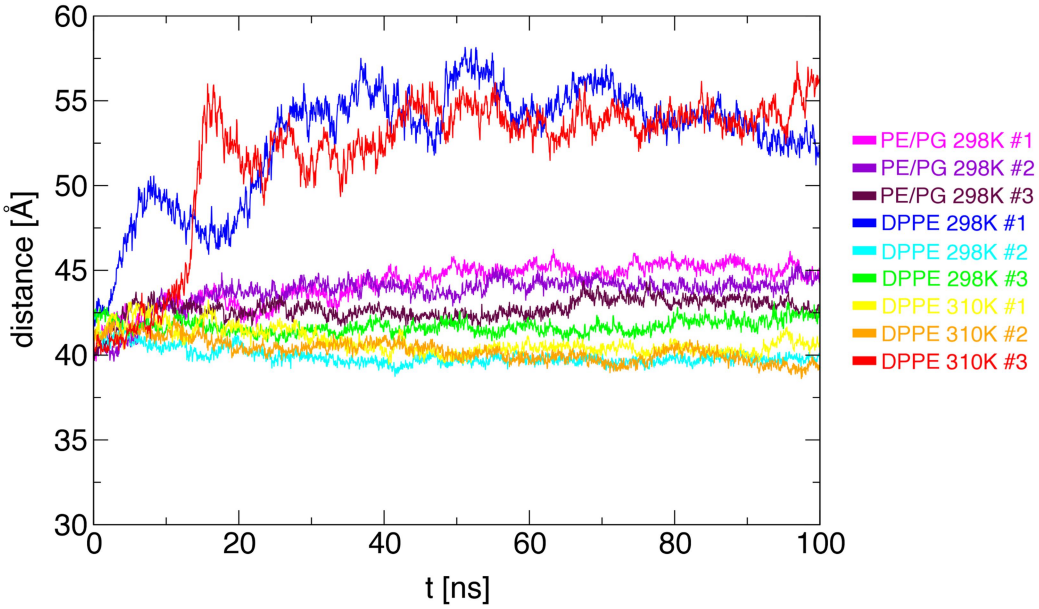

Fig. S10. Molecular dynamics results. Measured distance between the centers of mass of soluble and TM domain for each replica carried out in DPPE bilayer at 298 K and 310 K, and in the mixed PE/PG bilayer at 298 K. The red and blue curves show the opening of the *Nm*EptA conformation and separation of two domains respectively.

Bibliography

1. Takeshita S, Sato M, Toba M, Masahashi W, & Hashimoto-Gotoh T (1987) High-copy-number and low-copy-number plasmid vectors for lacZ alpha-complementation and chloramphenicol- or kanamycin-resistance selection. *Gene* 61(1):63-74.
2. Piek S*, et al.* (2014) The role of oxidoreductases in determining the function of the neisserial lipid A phosphoethanolamine transferase required for resistance to polymyxin. *PloS one* 9(9):e106513.
3. Kabsch W (2010) Xds. *Acta Crystallogr D Biol Crystallogr* 66(Pt 2):125-132.
4. Winn MD*, et al.* (2011) Overview of the CCP4 suite and current developments. *Acta Crystallogr D Biol Crystallogr* 67(Pt 4):235-242.
5. Emsley P, Lohkamp B, Scott WG, & Cowtan K (2010) Features and development of Coot. *Acta Crystallogr D Biol Crystallogr* 66(Pt 4):486-501.
6. Adams PD*, et al.* (2010) PHENIX: a comprehensive Python-based system for macromolecular structure solution. *Acta Crystallogr D Biol Crystallogr* 66(Pt 2):213-221.
7. Alexandrov AI, Mileni M, Chien EY, Hanson MA, & Stevens RC (2008) Microscale fluorescent thermal stability assay for membrane proteins. *Structure* 16(3):351-359.
8. Savitzky A & Golay M (1964) Smoothing and Differentiation of Data by Simplified Least Squares Procedures. *Analytical Chemistry* 36:1627.
9. Apicella MA, Griffiss JM, & Schneider H (1994) Isolation and characterization of lipopolysaccharides, lipooligosaccharides, and lipid A. *Methods Enzymol* 235:242-252.
10. Westphal O & Jann K (1965) Bacterial lipopolysaccharides. *Methods in Carbohydrate Chemistry* 5:83-91.
11. John CM*, et al.* (2012) Lack of lipid A pyrophosphorylation and functional lptA reduces inflammation by Neisseria commensals. *Infect Immun* 80(11):4014-4026.

12. Lehrer SS (1971) Solute Perturbation of Protein Fluorescence - Quenching of Tryptophyl Fluorescence of Model Compounds and of Lysozyme by Iodide Ion. *Biochemistry-Us* 10(17):3254-3263.

13. Wilkins MR*, et al.* (1997) Detailed peptide characterization using PEPTIDEMASS--a World-Wide-Web-accessible tool. *Electrophoresis* 18(3-4):403-408.

14. Van Der Spoel D*, et al.* (2005) GROMACS: fast, flexible, and free. *J Comput Chem* 26(16):1701-1718.

15. Schmid N*, et al.* (2011) Definition and testing of the GROMOS force-field versions 54A7 and 54B7. *Eur Biophys J* 40(7):843-856.

16. Piggot TJ, Holdbrook DA, & Khalid S (2011) Electroporation of the E. coli and S. Aureus membranes: molecular dynamics simulations of complex bacterial membranes. *The journal of physical chemistry. B* 115(45):13381-13388.

17. Domański J, Stansfeld PJ, Sansom MSP, & Beckstein O (2010) Lipidbook: A Public Repository for Force Field Parameters Used in Membrane Simulations. . *J. Membrane Biol.* 236:255-258.

18. Berendsen HJC, Postma JPM, van Gunsteren WF, & Hermans J (1981) Interaction Models for Water in Relation to Protein Hydration. *Intermolecular Forces. Proceedings of the Fourteenth Jerusalem Symposium on Quantum Chemistry and Biochemistry Held in Jerusalem, Israel, April 13 - 16, 1981*, ed Pullman B), Vol 14, pp 331-342.

19. Tironi IG, Sperb R, Smith PE, & van Gunsteren WF (1995) A Generalized Reaction Field Method for Molecular-Dynamics Simulations. *J Chem Phys* 102(13):5451-5459.

20. Hess B, Bekker H, Berendsen HJC, & Fraaije JGEM (1997) LINCS: A Linear Constraint Solver for Molecular Simulations. *J Comput Chem* 18(12):1463-1472.

21. Miyamoto S & Kollman PA (1992) SETTLE: An Analytical Version of the Shake and Rattle Algorithm for Rigid Water Models. *J Comput Chem* 13(8):952-962.

22. Berendsen HJC, Postma JPM, Vangunsteren WF, Dinola A, & Haak JR (1984) Molecular-Dynamics with Coupling to an External Bath. *J Chem Phys* 81(8):3684-3690.

23. Humphrey W, Dalke A, & Schulten K (1996) VMD - Visual Molecular Dynamics. *Journal of Molecular Graphics and Modelling* 14:33-38.

24. Cullen TW & Trent MS (2010) A link between the assembly of flagella and lipooligosaccharide of the Gram-negative bacterium Campylobacter jejuni. *Proceedings of the National Academy of Sciences of the United States of America* 107(11):5160-5165.

25. Arroyo LA*, et al.* (2011) The pmrCAB operon mediates polymyxin resistance in Acinetobacter baumannii ATCC 17978 and clinical isolates through phosphoethanolamine modification of lipid A. *Antimicrob Agents Chemother* 55(8):3743-3751.

26. Fage CD, Brown DB, Boll JM, Keatinge-Clay AT, & Trent MS (2014) Crystallographic study of the phosphoethanolamine transferase EptC required for polymyxin resistance and motility in Campylobacter jejuni. *Acta Crystallogr D Biol Crystallogr* 70(Pt 10):2730-2739.

27. Trombley MP*, et al.* (2015) Phosphoethanolamine Transferase LptA in Haemophilus ducreyi Modifies Lipid A and Contributes to Human Defensin Resistance In Vitro. *PloS one* 10(4):e0124373.

28. Tamayo R*, et al.* (2005) Identification of cptA, a PmrA-regulated locus required for phosphoethanolamine modification of the Salmonella enterica serovar typhimurium lipopolysaccharide core. *J Bacteriol* 187(10):3391-3399.

29. Lee H, Hsu FF, Turk J, & Groisman EA (2004) The PmrA-regulated pmrC gene mediates phosphoethanolamine modification of lipid A and polymyxin resistance in Salmonella enterica. *J Bacteriol* 186(13):4124-4133.

30. Reynolds CM, Kalb SR, Cotter RJ, & Raetz CR (2005) A phosphoethanolamine transferase specific for the outer 3-deoxy-D-manno-octulosonic acid residue of Escherichia coli lipopolysaccharide. Identification of the eptB gene and Ca2+ hypersensitivity of an eptB deletion mutant. *The Journal of biological chemistry* 280(22):21202-21211.

31. Kim SH, Jia W, Parreira VR, Bishop RE, & Gyles CL (2006) Phosphoethanolamine substitution in the lipid A of Escherichia coli O157 : H7 and its association with PmrC. *Microbiology* 152(Pt 3):657-666.

32. Sievers F, *et al.* (2011) Fast, scalable generation of high-quality protein multiple sequence alignments using Clustal Omega. *Mol Syst Biol* 7:539.

33. Kabsch W & Sander C (1983) Dictionary of protein secondary structure: pattern recognition of hydrogen-bonded and geometrical features. *Biopolymers* 22(12):2577-2637.

34. Bond CS & Schuttelkopf AW (2009) ALINE: a WYSIWYG protein-sequence alignment editor for publication-quality alignments. *Acta Crystallogr D Biol Crystallogr* 65(Pt 5):510-512.

35. Livingstone CD & Barton GJ (1993) Protein sequence alignments: a strategy for the hierarchical analysis of residue conservation. *Comput Appl Biosci* 9(6):745-756.

36. Wanty C, *et al.* (2013) The structure of the neisserial lipooligosaccharide phosphoethanolamine transferase A (LptA) required for resistance to polymyxin. *Journal of molecular biology* 425(18):3389-3402.

37. Trent MS & Raetz CRH (2002) Cloning of EptA, the lipid A phosphoethanolamine transferase associated with polymyxin resistance. . *Journal of Endotoxin Research* 8(3):158.

38. Liu YY, *et al.* (2016) Emergence of plasmid-mediated colistin resistance mechanism MCR-1 in animals and human beings in China: a microbiological and molecular biological study. *Lancet Infect Dis* 16(2):161-168.